energies

MDPI

Article

Bidirectional Power Flow Control of a Multi Input Converter for Energy Storage System

Cheng-Yu Tang [1,*] and Jun-Ting Lin [2]

1 Department of Electrical Engineering, National Taipei University of Technology, Taipei 10608, Taiwan
2 Department of Electrical Engineering, Feng-Chia University, Taichung 40724, Taiwan; deity840518@gmail.com
* Correspondence: cytang@ntut.edu.tw; Tel.: +886-2-2771-2171

Received: 9 September 2019; Accepted: 29 September 2019; Published: 30 September 2019

check for updates

Abstract: The objective of this paper is to propose a multi-input DC-DC converter with bidirectional power flow control capability. Compared to the traditional power converter, the multi-input converter (MIC) can save on the number of components and the circuit cost. Under normal conditions, the MIC is able to transfer energy from different input sources to the load. However, if the battery module is adopted, both the charging or discharging features should be considered. Therefore, the bidirectional power flow control of the MIC is necessary. On the other hand, because of the inconsistency characteristics of batteries, unbalanced circuit operation might occur whereby the circuit and the battery might be damaged. Therefore, dynamic current regulation strategies are developed for the MIC. Consequently, the proposed MIC circuit is able to achieve the bidirectional power flow control capability as well as control the input currents independently. Detailed circuit analysis and comprehensive mathematical derivation and of the proposed MIC will be presented in this paper. Finally, both simulation and experimental results obtained from a 500 W prototype circuit verify the performance and feasibility of the proposed bidirectional multi-input converter.

Keywords: multi-input converter; bidirectional power flow control; energy storage system

1. Introduction

Nowadays, global environmental protection and green energy sources are being paid high attention to deal with the fossil fuel usage and carbon dioxide emission issues [1,2]. Novel energy technologies such as photovoltaic (PV) power generation systems, wind power systems, electric vehicles and advanced consumer electronics have been rapidly developed [3–6]. The battery module is an essential component for energy storage [7–10]. In addition, a battery charger consisting of DC-DC converters integrated with the pulse-width-modulation (PWM) technology is necessary to control the battery energy [11–13]. Moreover, the bidirectional power flow control of the battery charger is also an essential function to realize both charging and discharging ability for the battery [14–17].

If two different sources are considered and expected to connect to the same load, two DC-DC converters should be utilized, as seen in the conceptual diagram shown in Figure 1a, where if the two input sources, V_{in1} and V_{in2} are replaced by battery modules, the charging or discharging current can be controlled independently via the two DC-DC converters. However, the number of required DC-DC converters will increase if more input sources are adopted. Consequently, the size and cost of the system will be increased while the stability will be decreased. In order to reduce the size and cost of the system as well as to enhance the circuit stability, the multi-input converter (MIC) has been developed with the circuit diagram shown in Figure 1b. It can be confirmed that two or more input sources can be included with one shared DC-DC converter. Moreover, the DC sources can be connected either in series or in parallel to transfer energy to the load via the MIC.

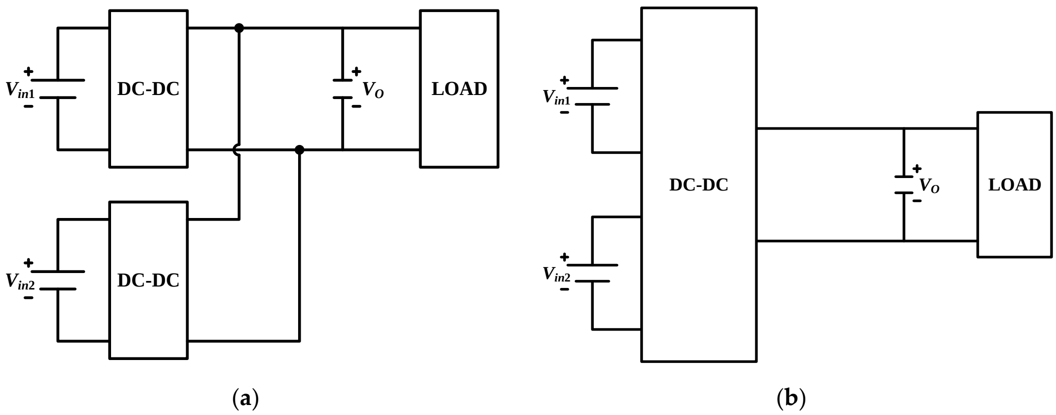

Figure 1. Conceptual diagrams of the (**a**) Distributed DC-DC converters; (**b**) Multi-input DC-DC converter.

Different kinds of MIC circuit topologies and applications have been proposed [18–23]. First, a multi-input DC-DC converter based on flux additivity was proposed in [18]. A multi-winding transformer was adopted in this MIC topology. Reference [19] proposed a MIC for the photovoltaic (PV) power system and AC mains applications with maximum power point tracking, power factor correction and ripple-free input current features. In [20], a novel double-input pulse-width-modulation DC-DC converter for high-/low-voltage sources is proposed. The two input sources can be connected either in series or in parallel to transfer the energy to the load. Besides, a multi-input inverter for the grid-connected hybrid photovoltaic/wind power system is proposed in [21]. The output power characteristics of the PV array and the wind turbine are also considered. Reference [22] proposed a general approach for developing multi-input converters (MICs). In this literature, it was confirmed that all of the MIC topologies can be summarized as two families, which are: (1) PVSCs and (2) PCSCs. In addition, a semi-isolated MIC for hybrid PV/wind power charger system was presented in [23], with a topology composed of isolated and/or non-isolated DC-DC converters. Although these proposed circuits and methods are effective, battery charging applications and the bidirectional power flow control are not considered and discussed.

Therefore, the aim of this paper is to propose a multi-input DC-DC converter with bidirectional power flow control ability for energy storage applications. The novelty and main features of this paper can be summarized as follows: (1) Four power switches with synchronous rectification feature are included in the MIC circuit to enhance the control flexibility as well as to improve the circuit efficiency; (2) the bidirectional power flow control with both charging and discharging capability are realized; (3) the dynamic current regulation are proposed and developed to control the input currents independently. The circuit modeling and comprehensive mathematical derivartions of the proposed bidirectional MIC circuit are also presented. Eventually, the performance and feasibility of the proposed bidirectional MIC topology and control strategies will be verified by both simulation and experimental results of a 500 W prototype circuit.

2. Circuit Configurations and Equivalent Models

2.1. Circuit Diagrams of the Proposed Bidirectional MIC

The circuit diagram of the proposed bidirectional multi-input DC-DC converter is shown in Figure 2. Four power switches integrated with one inductor and one capacitor are included in the circuit. The input ports of the converter are connected to two DC source whereas the output port will be connected to the DC load. It should be mentioned that different from the circuit topology presented in [19], two power switches, S_3 and S_4, are utilized to replace the rectifying diodes as well as to enhance control feasibilities. Therefore, the synchronous rectification function will be achieved for the four power switches. Moreover, if DC loads are adopted for the input ports while the DC source is utilized for the output port, the proposed MIC can transfer the power from the other direction. As a result, the bidirectional power flow control can be realized.

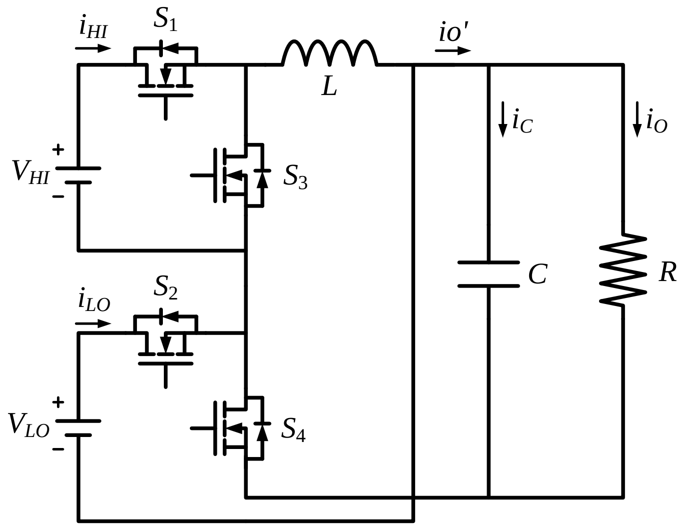

Figure 2. The circuit diagram of the multi-input step-up/step-down converter.

2.2. Analyzation of Different Equivalent Models

Compared to the MIC circuit in [20], in the proposed circuit the rectifying diodes are replaced by two power switches. Therefore, the synchronous rectification should be considered. With the synchronous rectification feature, the bidirectional power flow control can be realized whereas the circuit efficiency can be increased. Besides, in general control of complex systems, introduction of switching has been intensively studied in coordination [24,25]. In the following, different circuit operation modes should be analyzed according to different switching combinations. In order to simplify the control, the upper side switches, S_1 and S_3, are controlled with synchronous rectification whereas the lower side switches, S_2 and S_4, are controlled with synchronous rectification. According to different switching states, seven operation modes can be obtained and described as follows:

- ➢ Mode I: The equivalent circuit of Mode I is shown in Figure 3a. In this mode, S_1 and S_2 are turned on while S_3 and S_4 are off. In the meantime, V_{in1} and V_{in2} are in series to charge the inductor, L. The demanded load energy is supplied from the capacitor, C.
- ➢ Mode II: During this state, S_1 and S_4 conduct. S_2 and S_4 are off. V_{in1} charges L and C by S_1 and S_4 as well as provide energy to the load, as shown in Figure 3b.
- ➢ Mode III: The equivalent circuit of this mode is shown in Figure 3c. In this mode, S_2 and S_3 are turned on while S_1 and S_4 are turned off. V_{in1} charges L whereas the load energy is supplied by C.
- ➢ Mode IV: Figure 3d shows the equivalent circuit of Mode IV. Under this mode, V_{in1} and V_{in2} will not transfer energy due to the off state of S_1 and S_2. In the same time, S_3 and S_4 are turned on and the demanded load energy can be obtained from L and C.
- ➢ Mode V: In this mode, S_3 and S_4 are turned on while S_1 and S_2 are turned off. L and C are charged by V_{DC}, as shown in Figure 3e.
- ➢ Mode VI: Figure 3f shows the equivalent circuit of Mode VI. Under this condition, S_2 and S_3 are off. V_{DC} charges L, C and V_{in1} in the same by S_1 and S_4.
- ➢ Mode VII: Under this mode, S_1 and S_4 are off. V_{DC} charges L, C and V_{in2} in the same by S_2 and S_3. The equivalent circuit of Mode VII is shown in Figure 3g.

It is worth mentioning that with the combination of Mode I, Mode II, Mode III and Mode IV, the MIC can transfer energy from input sources to the output load. In this paper, these fours modes are defined as the discharging scenario.

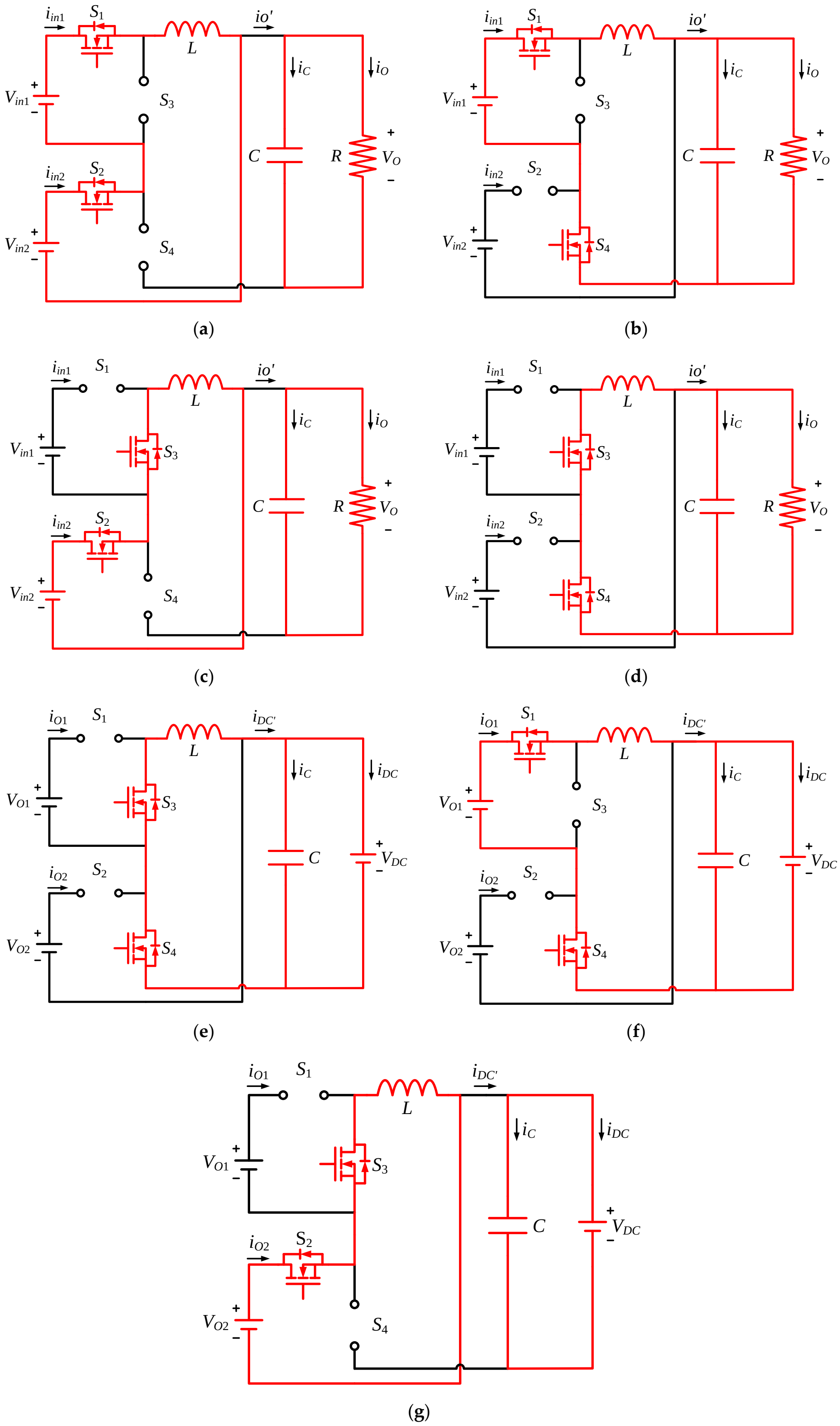

Figure 3. Equivalent circuits of different operation modes (**a**) Mode I; (**b**) Mode II; (**c**) Mode III; (**d**) Mode IV; (**e**) Mode V; (**f**) Mode VI; (**g**) Mode VII.

On the other hand, if R is replaced by a DC source, V_{DC}, the energy can be transferred from V_{DC} to V_{in1} and V_{in2} via the combination of Mode V, Mode VI and Mode VII. Therefore, the operation of these three modes are defined as charging scenario. As a result, the bidirectional power flow control capability of the MIC can be realized by these seven operation modes.

3. Circuit Operation Principles and the Proposed Bidirectional Power Flow Control

Detailed circuit operation principles and the bidirectional power flow control will be presented in this section. First, all circuit elements are considered as ideal without parasitic components. The MIC will be operated in the continuous conduction mode (CCM). In addition, the resistive load is utilized for the output port in both charging and discharging scenarios.

3.1. The Discharging Scenario

In the discharging scenario, V_{in1} and V_{in2} are defined as input ports whereas V_{in1} is set to be larger than V_{in2}. Therefore, the duty ration of S_1 should be greater than the duty ration of S_2. On the other hand, with the synchronous rectification, S_3 and S_4 will be the complementary PWM signals of S_1 and S_2, respectively. PWM signal waveforms of the four power switches under the discharging scenario are shown in Figure 4.

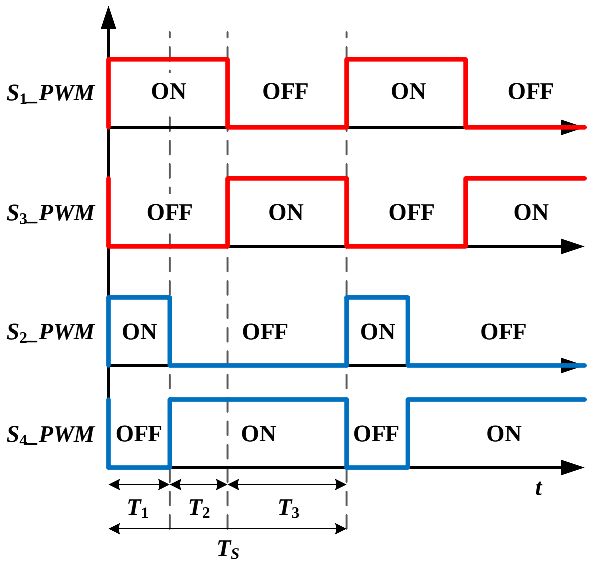

Figure 4. PWM signal waveforms of the power switches under the discharging scenario.

By adopting the PWM control concept shown in Figure 4 as well as combining Mode I, Mode II and Mode IV shown in Figure 3, theoretical waveforms of the discharging scenario can be obtained, as shown in Figure 5. In Figure 5, V_{GS1} and V_{GS2} represent the gate signals of S_1 and S_2, respectively. It should be mentioned that the gate signals of S_3 and S_4 will be the complementary waveforms of S_1 and S_2 and which are not revealed in Figure 5. V_L and i_L are the inductor voltage and current, respectively. i_{in1} and i_{in2} are the input currents of V_{in1} and V_{in2}, respectively. $i_O{}'$ is the output current before the capacitor, C, whereas i_C is the current flow into the capacitor. In the following, three intervals of T_1, T_2 and T_3 will be distinguished from one switching cycle to analyze the MIC circuit.

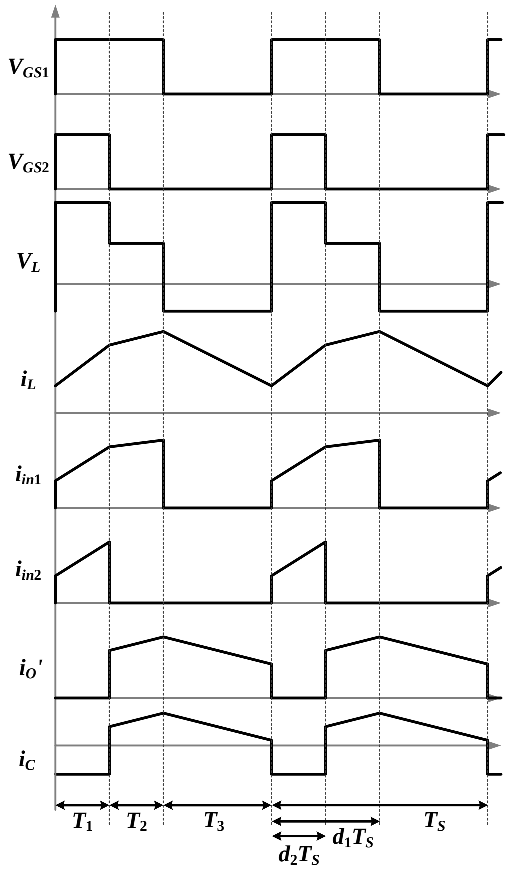

Figure 5. Theoretical waveforms of the discharging scenario.

In the T_1 period, the MIC circuit is operated in Mode I. The inductor, L, is charged by both of the two input sources. Therefore, the inductor voltage, V_L, will be equal to the summation of V_{in1} and V_{in2}, as shown in Equation (1). Besides, T_1 will be equal to the conduction time of S_2, as Equation (2) shows:

$$V_L = V_{in1} + V_{in2} \quad (1)$$

$$T_1 = d_2 T_S, \quad (2)$$

where d_2 is the duty cycle of S_2 and T_S represents the switching period.

During the T_2 interval, the MIC circuit is operated in Mode II. V_L will be the difference of V_{in1} and V_O, as Equation (3) shows. In addition, the conduction time of T_2 can be written as Equation (4):

$$V_L = V_{in1} - V_O \quad (3)$$

$$T_2 = (d_1 - d_2) T_S \quad (4)$$

where d_1 is the duty cycle of S_1.

For the T_3 interval, the MIC circuit is operated in Mode IV. In the meantime, V_L and T_3 can be calculated as:

$$V_L = -V_O \quad (5)$$

$$T_3 = (1 - d_1) T_S \quad (6)$$

According to the volt-second balance theory, the increasing amount of the inductor current, ΔI_{ON}, will be equal to the decreasing amount of the inductor current, ΔI_{OFF}, within one switching period, as:

$$\Delta I_{ON} = \Delta I_{OFF} \quad (7)$$

With the volt-second balance principle of the inductor, Equation (7) can be modified as:

$$\Delta V_{ON} \times T_{ON} = \Delta V_{OFF} \times T_{OFF} \tag{8}$$

where ΔV_{ON} and ΔV_{OFF} are the changing amount of inductor voltage during the conduction period, T_{ON}, and the cut off period, T_{OFF}, respectively.

In Equation (8), ΔV_{ON} can be obtained from the inductor derived in Equations (1) and (3). T_{ON} can be obtained from T_1 and T_2 shown Equations (2) and (4). ΔV_{OFF} will be equal to the voltage shown in Equation (5). T_{OFF} can be expressed as T_3 shown in Equation (6). Therefore, by the combination from Equations (1) to (6), Equation (8) can be expressed as:

$$d_2 T_S(V_{in1} + V_{in2}) + (d_1 - d_2)T_S(V_{in1} - V_O) = (1 - d_1)T_S(V_O). \tag{9}$$

Eventually, by the rearrangement of Equation (9), the output voltage, V_O, can be derived as Equation (10). It can be confirmed that with proper control of d_1 and d_2, V_O can be regulated with a function of V_{in1} and V_{in2}:

$$V_O = \frac{d_1}{1 - d_2} V_{in1} + \frac{d_2}{1 - d_2} V_{in2}. \tag{10}$$

In addition, if d_2 larger than d_1, Equation (9) should be modified as:

$$d_1 T_S(V_{in1} + V_{in2}) + (d_2 - d_1)T_S V_{in2} + (1 - d_2)T_S(-V_O) = 0. \tag{11}$$

However, if Equation (11) is rearranged, the output voltage will be the same as V_O shown in Equation (10). Therefore, the two input sources, V_{in1} and V_{in2} can be controlled independently.

On the other hand, the input currents, I_{in1} and I_{in2} will be equal to the inductor current, I_L, when S_1 or S_2 conducts. Therefore, I_{in1} and I_{in2} can be expressed as:

$$I_{in1} = d_1 \times I_L \tag{12}$$

$$I_{in2} = d_2 \times I_L. \tag{13}$$

Besides, the output current, I_O, can be written as:

$$I_O = (1 - d_2)I_L. \tag{14}$$

As a result, by the rearrangement of Equations (12)–(14), relations between the input currents and the output current can be derived as:

$$I_{in1} = \left(\frac{d_1}{1 - d_2}\right)I_O \tag{15}$$

$$I_{in2} = \left(\frac{d_2}{1 - d_2}\right)I_O \tag{16}$$

3.2. The Charging Scenario

In the charging scenario, Mode V, Mode VI and Mode VII will be adopted. In Figure 3, it can be confirmed that a DC source, V_{DC}, is used to replace R and determined as the input port. On the contrary, V_{O1} and V_{O2} are defined as output ports. Besides, two charging scenarios can be defined, which are: (1) the charging scenario A and (2) the charging scenario mode B. In the following, the two different charging scenarios will be described individually.

3.2.1. The Charging Scenario A

For the charging scenario A, Mode V and Mode VI are utilized to transfer the energy from V_{DC} to V_{O1}. The equivalent circuit diagram of this scenario is shown in Figure 6a. The conceptual diagram of PWM control signals is shown in Figure 7a whereas theoretical waveforms of the charging scenario A are shown in Figure 8a. V_{GS1} and V_{GS2} are the gate signals of S_1 and S_2, respectively. i_{O1} and i_{O2} are the output currents. i_{O1}' is the current before C_{O1} whereas i_{CO1} is the C_{O1} capacitor current. In the following, interval T_1 and T_2 are distinguished from one switching cycle to analyze this scenario.

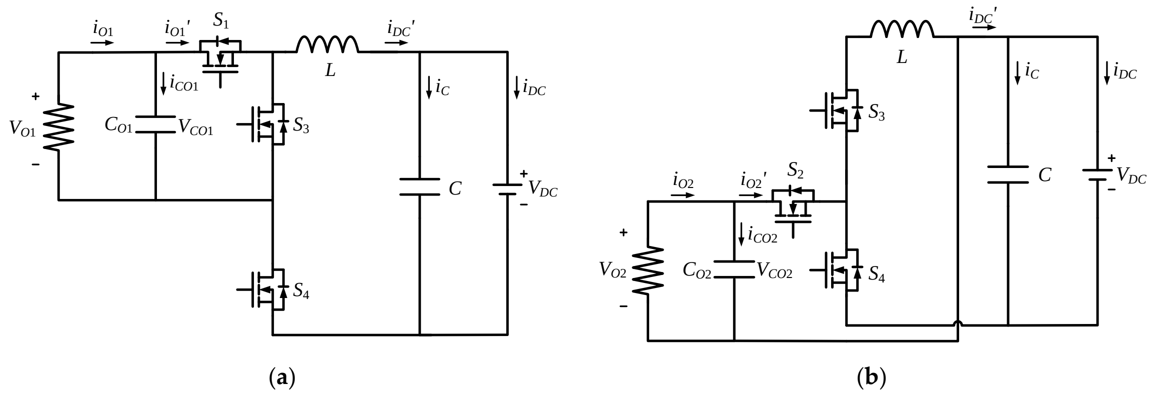

Figure 6. Equivalent circuit diagrams of (**a**) The charging scenario A; (**b**) The scenario mode B.

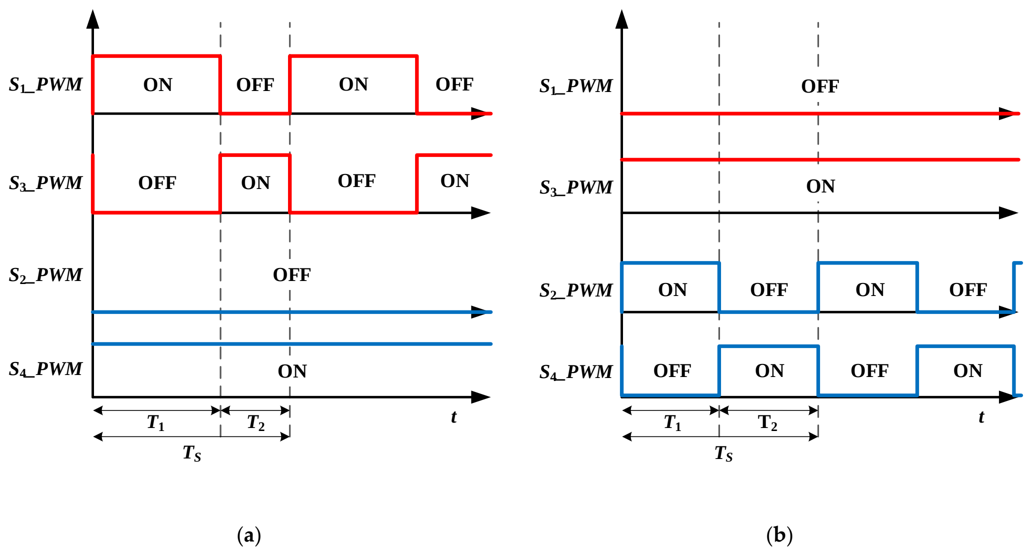

Figure 7. PWM signals of (**a**) The charging scenario A; (**b**) The charging scenario B.

During the T_1 period, the MIC circuit is operated in Mode VI. In the meantime, V_L will be the difference of V_{O1} and V_{DC}, as shown in Equation (17). Besides, T_1 will be equal to the conduction time of S_1, as Equation (18) shows:

$$V_L = V_{O1} - V_{DC} \tag{17}$$

$$T_1 = d_1 T_S. \tag{18}$$

In the T_2 interval, the MIC circuit is operated in Mode V. V_L is equal to V_{DC}, as Equation (19) shows. In addition, the conduction time of T_2 can be written as Equation (20).

$$V_L = V_{DC} \tag{19}$$

$$T_2 = (1 - d_1) T_S. \tag{20}$$

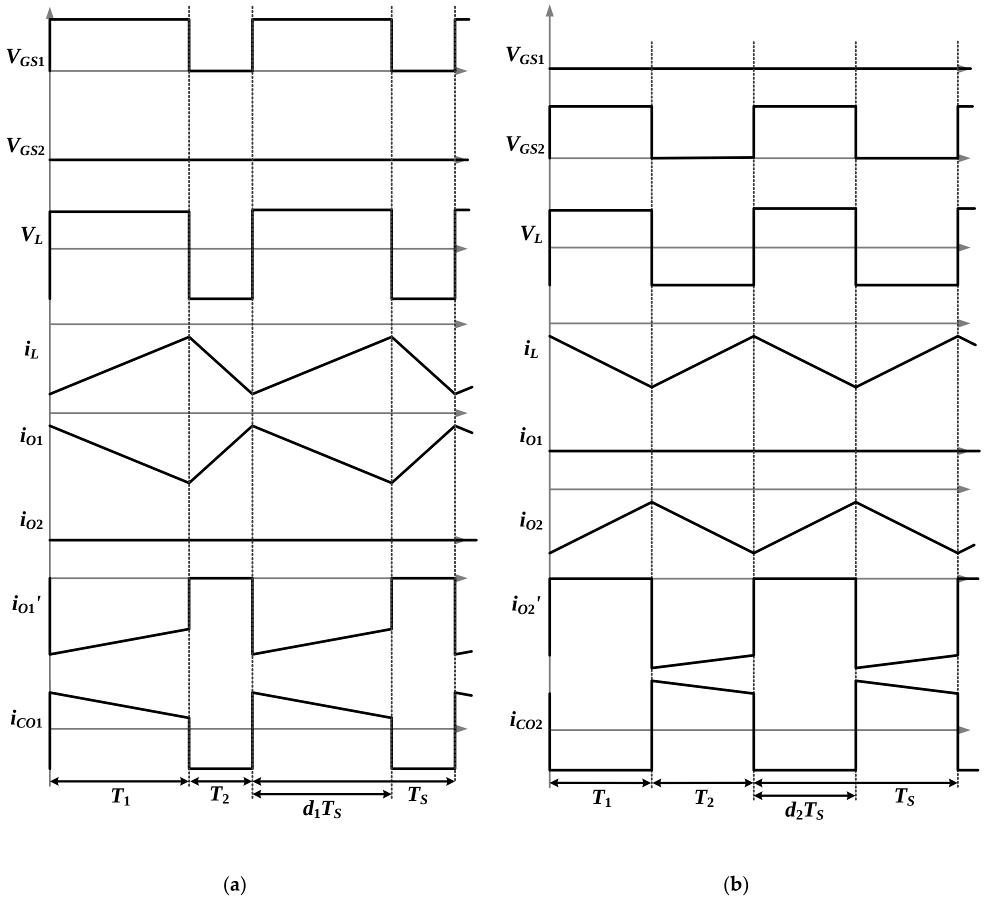

Figure 8. Theoretical waveforms of (**a**) The charging scenario A; (**b**) The charging scenario B.

By the combination of Equations (17)–(20), Equation (21) can be obtained as:

$$d_1 T_S (V_{O1} - V_{DC}) = (1 - d_1) T_S V_{DC}. \tag{21}$$

After the simplification, Equation (21) can be modified as:

$$V_{DC} = d_1 V_{O1}. \tag{22}$$

From Equation (22), it can be confirmed that the MIC in this scenario will be operated as a conventional DC-DC boost converter.

3.2.2. The Charging Scenario B

If the charging scenario B is considered, Mode V and Mode VII should be adopted. The equivalent circuit diagram of this scenario is shown in Figure 6b. The conceptual diagram of PWM control signals is shown in Figure 7b. Theoretical waveforms of the charging scenario B are shown in Figure 8b. V_{GS1} and V_{GS2} are the gate signals of S_1 and S_2, respectively. i_{O1} and i_{O2} are the output currents. i_{O2}' is the current before C_{O2} whereas i_{CO2} is the C_{O2} capacitor current. In the following, interval T_1 and T_2 are distinguished from one switching cycle to analyze this scenario.

During the T_1 period, the MIC circuit is operated in Mode VII. V_L is equal to the output voltage, V_{O2}, as shown in Equation (23). Besides, T_1 will be equal to the conduction time of S_2, as Equation (24) shows:

$$V_L = V_{O2} \tag{23}$$

$$T_1 = d_2 T_S. \tag{24}$$

In the T_2 interval, the MIC circuit is operated in Mode V. V_L is equal to V_{DC}, as Equation (25) shows. In addition, the conduction time of T_2 can be written as Equation (26):

$$V_L = V_{DC} \tag{25}$$

$$T_2 = (1 - d_2)T_S. \tag{26}$$

By the combination of Equations (23)–(26), Equation (27) can be written as:

$$d_2 T_S V_{O2} = (1 - d_2)T_S V_{DC}. \tag{27}$$

Eventually, Equation (27) can be derived as:

$$V_{O2} = \frac{1 - d_2}{d_2} V_{DC}. \tag{28}$$

From Equation (28), it can be confirmed that the MIC in this scenario will be operated as a conventional DC-DC buck-boost converter.

4. Simulation and Experimental Validations

In order to verify the performance and feasibility of the proposed bidirectional MIC, a 500 W prototype circuit is designed and implemented. The specifications of the circuit are shown in Table 1. The inductance, L is determined as 100 µH. The capacitance of C, C_{in1} and C_{in2} are calculated as 470 µF, 330 µF and 470 µF, respectively. The MOSFET, IRF640N, is chosen as main switches, whereas the switching frequency is determined as 50 kHz. The gate drive IC, TLP250 is used to drive the power switches. It is worth mentioning that the DSP TMS320F28335 made by Texas Instruments is utilized as the system controller. It is worth mentioning that all components of the circuit are assumed to be functional while he robustness consideration can be found in [26,27]. In the following, both simulation and experimental results are presented.

Table 1. Circuit specifications of the proposed bidirectional MIC.

Parameters	Value or Type
Rated power	500 W
Inductance of L	100 µH
Capacitance of C	470 µF
Capacitance of C_{in1}	330 µF
Capacitance of C_{in2}	470 µF
Switches of S_1, S_2, S_3 and S_4	MOSFET IRF640N
Switching frequency	50 kHz
Gate driver IC for the switches	TLP250
System controller	TI DSP TMS320F28335

4.1. Simulation Results

The proposed bidirectional MIC are first verified via the Matlab/Simulink with the circuit diagrams shown in Figure 9. Simulation results of the discharging scenario are shown in Figure 10. Two cases are simulated to illustrate the discharging scenario. Figure 10a shows waveforms of the I_{in1}, I_{in2}, I_O and V_O of case I. In this case, I_{in1} is set as 1 A and I_{in2} is set as 6 A in the beginning. At t = 0.3 s, I_{in1} is increased to 2 A. In order to remain the constant I_O and V_O, I_{in2} will be decreased by the controller. Besides, Figure 10b shows waveforms of the I_{in1}, I_{in2}, I_O and V_O of case II. In this case, I_{in1} is set as 6 A and I_{in2} is set as 1 A in the beginning. During t = 0.3 s, I_{in2} is increased to 2 A whereas I_{in1} is decreased by the controller to remain the constant I_O and V_O. In other words, the dynamic input current regulation can be achieved. It should be mentioned that I_O and V_O are determined as 5 A and 50 V, respectively.

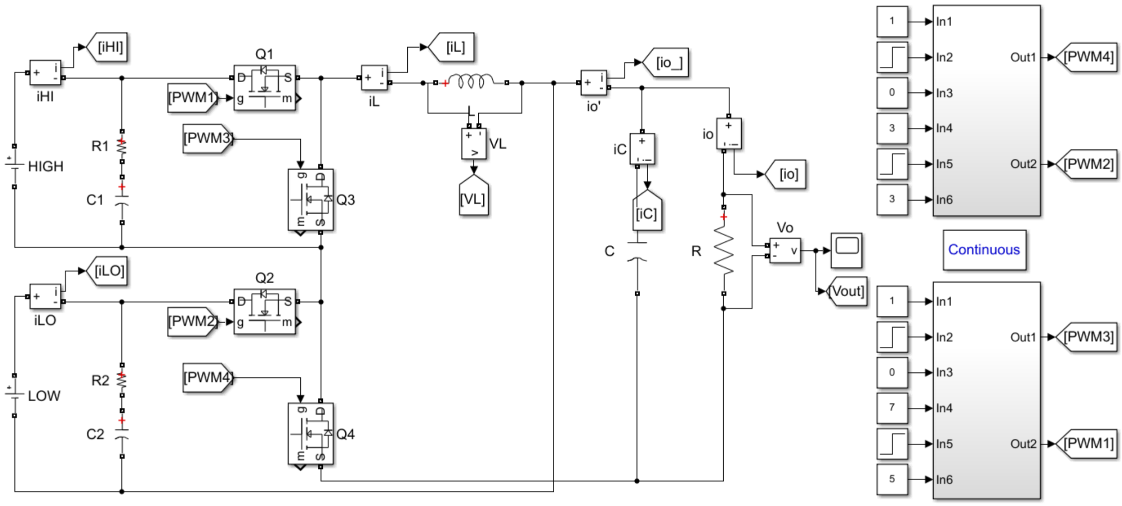

Figure 9. Circuit diagrams of the proposed bidirectional MIC in Matlab/Simulink.

On the other hand, simulation results of the charging scenario are shown in Figure 11. Figure 11a shows the results of V_{DC}, I_{DC}, V_{O1} and I_{O1} under the charging scenario A. In this case, V_{DC} and I_{DC} are set as 50 V and −20 A, respectively. V_{O1} and I_{O1} are set as 100 V and −10 A, respectively. Under this case, the MIC is operated as a boost converter. Simulation results of V_{DC}, I_{DC}, V_{O2} and I_{O2} under the charging scenario B are shown in Figure 11b. In this case, both V_{DC} and V_{O2} are set as 50 V while both I_{DC} and I_{O2} are set as −10 A. It is worth mentioning that the MIC is acted as a buck-boost converter under this scenario.

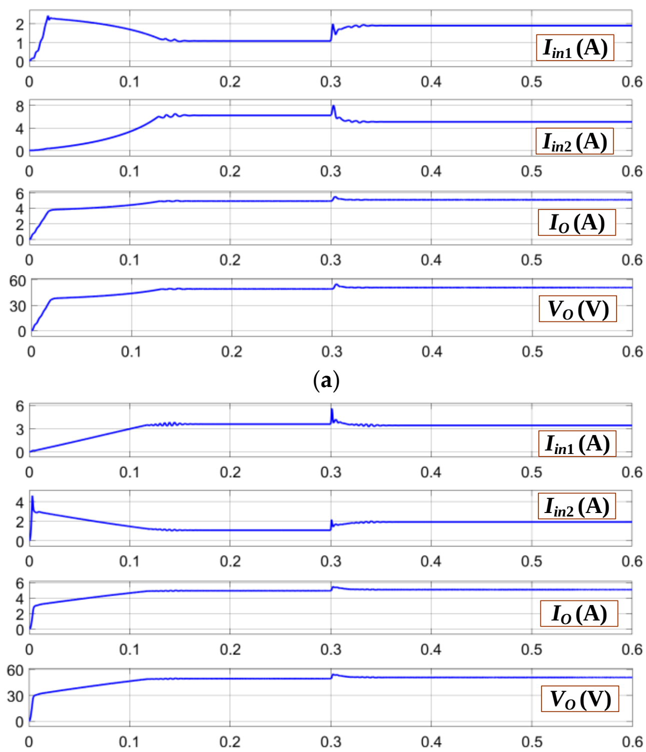

Figure 10. Simulation results of the discharging scenario (**a**) Case I; (**b**) Case II.

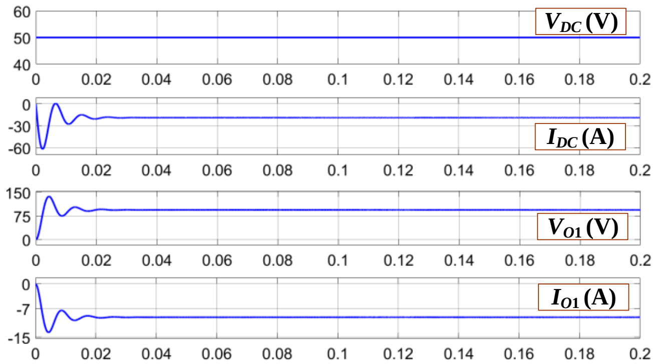

(**a**)

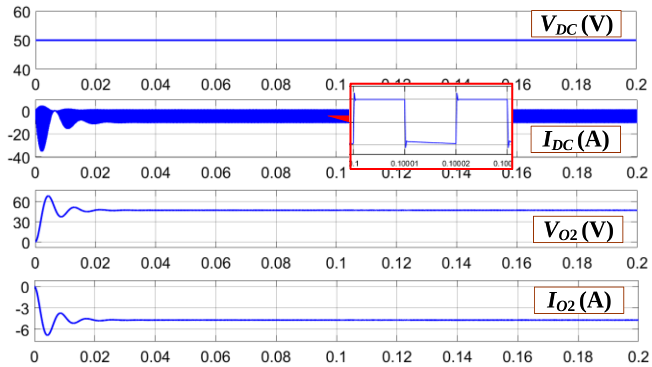

(**b**)

Figure 11. Simulation results of (**a**) The charging scenario A; (**b**) The charging scenario B.

4.2. Experimental Validations

In this section, experimental results of the bidirectional MIC will be presented. First, the prototype circuit figure of the MIC is shown in Figure 12a. It can be seen that the main circuit, the ASC712 and amplifier circuit and the DSP TMS320F28335 are included. In addition, the gate signal waveforms, V_{GS1}, V_{GS2} and the inductor current waveform, I_L of the discharging scenario are shown in Figure 12b. The gate signal waveforms, V_{GS1}, V_{GS3} and the inductor current waveform, I_L of the charging scenario A are shown in Figure 12c. The gate signal waveforms, V_{GS2}, V_{GS4} and the inductor current waveform, I_L of the charging scenario B are shown in Figure 12d.

On the other hand, Figure 13 demonstrates the experimental results under the same conditions of shown in Figures 10 and 11, respectively. First, Figure 13a shows experimental waveforms of case I. At $t = t_1$, I_{in1} is increased. In order to remain the power flow balance, I_{in2} should be decreased. Therefore, it can be seen that I_O and V_O are well regulated as constant values. On the contrary, Figure 13b demonstrate the opposite scenario of Figure 13a. In Figure 13b, I_{in1} is decreased at $t = t_1$. In the meantime, I_{in2} should be increased to maintain the power flow balance. As a result, I_O and V_O are well stabilized in a constant value.

Moreover, experimental waveforms of V_{DC}, I_{DC}, V_{in1} and I_{in1} with the charging scenario A are shown in Figure 13c whereas experimental waveforms of V_{DC}, I_{DC}, V_{in2} and I_{in2} with the charging scenario B are shown in Figure 13d.

According to the simulation and experimental waveforms, the steady-state operation, dynamic current regulation and the bidirectional power flow control capability of the proposed MIC circuit are verified.

Finally, Figure 14 shows the circuit efficiency of the proposed MIC under different load condition. It can be confirmed that the peak efficiency is about 87%. It should be mentioned that the efficiency from 10% to 70% load are measured by the experiments of the prototype MIC circuit. However, because of the limitation of the experimental equipment, the efficiency of 80%, 90% and 100% load operation are calculated and estimated. In the future work, the soft-switching function can be included for the MIC to further improve the circuit efficiency.

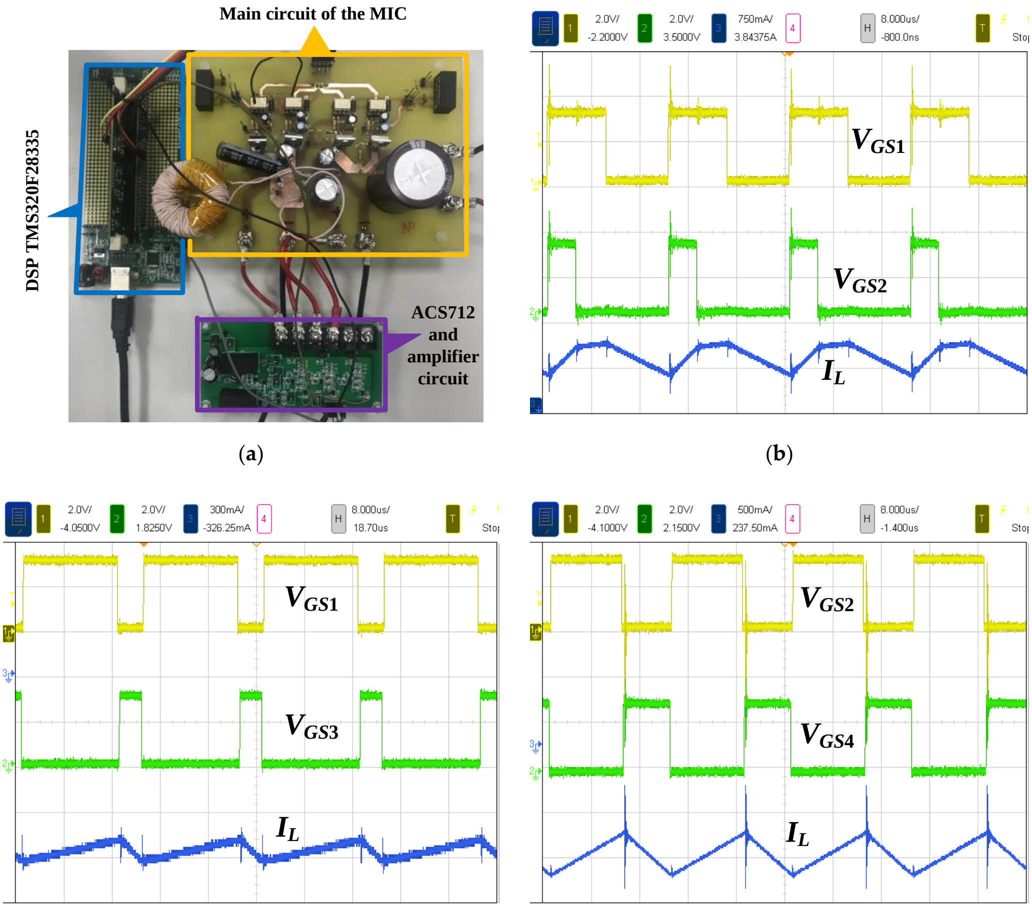

(**a**) (**b**)

(**c**) (**d**)

Figure 12. The hardware circuit figure and experimental waveforms (**a**) The prototype circuit figure; (**b**) The gate signal and inductor current waveforms with the discharging scenario; (**c**) The gate signal and inductor current waveforms with the charging scenario A; (**d**) The gate signal and inductor current waveforms with the charging scenario B.

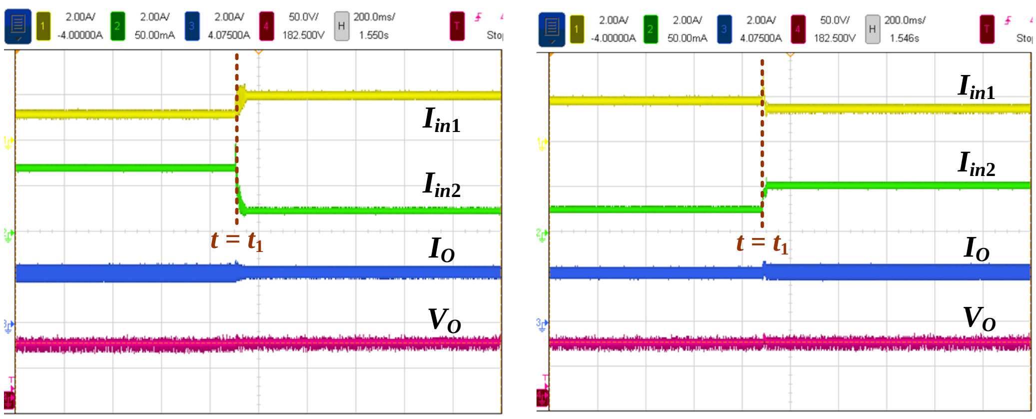

(**a**) (**b**)

Figure 13. *Cont.*

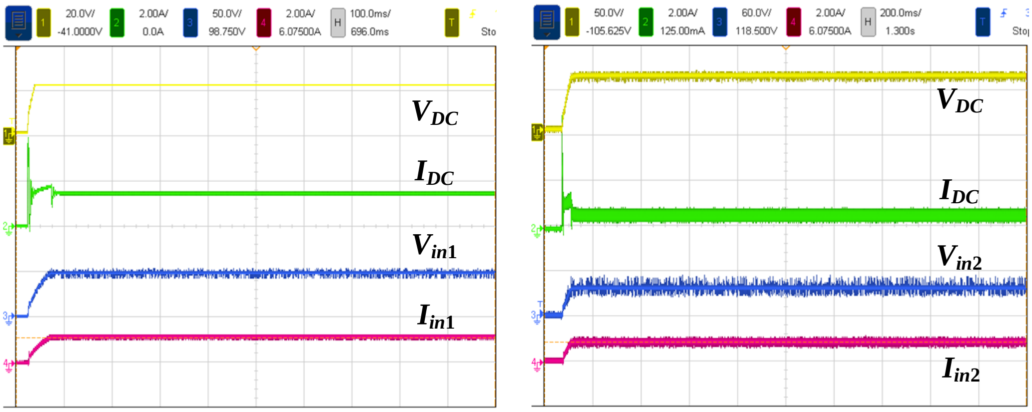

(**c**) (**d**)

Figure 13. Experimental results of (**a**) The discharging scenario, case I; (**b**) The discharging scenario, Case II; (**c**) The charging scenario A; (**d**) The charging scenario B.

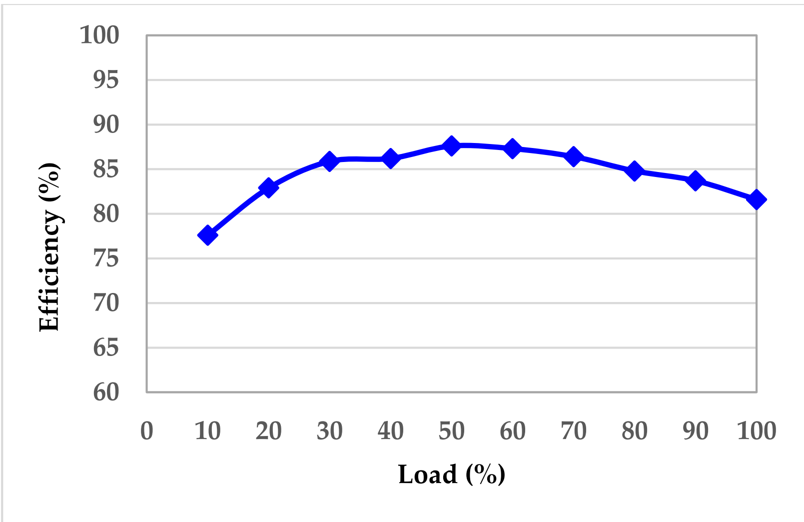

Figure 14. Experimental efficiency measurement of the proposed MIC circuit.

5. Conclusions

A multi-input DC-DC converter with bidirectional power flow control feature is proposed in this paper. The main features of the MIC circuit can be summarized as follows: (1) Two power switches are utilized to replace diodes as well as to achieve the synchronous rectification; (2) The bidirectional power flow control with both charging and discharging capability are realized; (3) The dynamic current regulation are developed to control the input currents independently as well as to stabilize the output voltage and current. Moreover, detailed circuit analysis, the circuit modeling and comprehensive mathematical derivartions of the proposed bidirectional MIC circuit are also presented. Finally, both simulation results and hardware experiments obtained from a 500 W circuit demonstrate the performance and feasibility of the proposed bidirectional MIC. In the future, the soft-switching technology can be adopted for the proposed MIC further increase the circuit efficiency.

Author Contributions: Conceptualization, C.-Y.T. and J.-T.L.; methodology, C.-Y.T. and J.-T.L.; software, J.-T.L.; validation, J.-T.L.; formal analysis, C.-Y.T. and J.-T.L.; investigation, C.-Y.T.; resources, C.-Y.T.; data curation, J.-T.L.; writing—original draft preparation, C.-Y.T.; writing—review and editing, C.-Y.T.; visualization, C.-Y.T.; supervision, C.-Y.T.; project administration, C.-Y.T.; funding acquisition, C.-Y.T.

Funding: This research received no external funding.

Conflicts of Interest: The authors declare no conflict of interest.

References

1. Zhuang, P.; Liang, H.; Pomphrey, M. Stochastic multi-timescale energy management of greenhouses with renewable energy sources. *IEEE Trans. Sustain. Energy* **2019**, *10*, 905–917. [CrossRef]
2. Leithon, J.; Sun, S.; Lim, T.J. Demand response and renewable energy management using continuous-time optimization. *IEEE Trans. Sustain. Energy* **2018**, *9*, 991–1000. [CrossRef]
3. Tang, C.; Kao, L.; Chen, Y.; Ou, S. Dynamic power decoupling strategy for three-phase PV power systems under unbalanced grid voltages. *IEEE Trans. Sustain. Energy* **2019**, *10*, 540–548. [CrossRef]
4. Tang, C.; Chen, Y.; Chen, Y. PV power System with multi-mode operation and Llow-voltage ride-through capability. *IEEE Trans. Ind. Electron.* **2015**, *62*, 7524–7533. [CrossRef]
5. Azizivahed, A.; Naderi, E.; Narimani, H.; Fathi, M.; Narimani, M.R. A new bi-objective approach to energy management in distribution networks with energy storage systems. *IEEE Trans. Sustain. Energy* **2018**, *9*, 56–64. [CrossRef]
6. Wu, F.; Li, X.; Feng, F.; Gooi, H.B. Multi-topology-mode grid-connected inverter to improve comprehensive performance of renewable energy source generation system. *IEEE Trans. Power Electron.* **2017**, *32*, 3623–3633. [CrossRef]
7. Zhang, Z.; Cai, Y.; Zhang, Y.; Gu, D.; Liu, Y. A distributed architecture based on microbank modules with self-reconfiguration control to improve the energy efficiency in the battery energy storage system. *IEEE Trans. Power Electron.* **2016**, *31*, 304–317. [CrossRef]
8. Saez-de-Ibarra, A.; Martinez-Laserna, E.; Stroe, D.; Swierczynski, M.; Rodriguez, P. Sizing study of second life Li-ion batteries for enhancing renewable energy grid integration. *IEEE Trans. Ind. Appl.* **2016**, *52*, 4999–5008. [CrossRef]
9. Varajão, D.; Araújo, R.E.; Miranda, L.M.; Lopes, J.A.P. Modulation strategy for a single-stage bidirectional and isolated AC–DC matrix converter for energy storage systems. *IEEE Trans. Ind. Electron.* **2018**, *65*, 3458–3468. [CrossRef]
10. El Mejdoubi, A.; Chaoui, H.; Gualous, H.; Van Den Bossche, P.; Omar, N.; Van Mierlo, J. Lithium-ion batteries health prognosis considering aging conditions. *IEEE Trans. Power Electron.* **2019**, *34*, 6834–6844. [CrossRef]
11. Kushwaha, R.; Singh, B. Power factor improvement in modified bridgeless landsman converter fed EV battery charger. *IEEE Trans. Veh. Technol.* **2019**, *68*, 3325–3336. [CrossRef]
12. Lee, I. Hybrid DC–DC converter with phase-shift or frequency modulation for NEV battery charger. *IEEE Trans. Ind. Electron.* **2016**, *63*, 884–893. [CrossRef]
13. Qu, X.; Chu, H.; Wong, S.; Tse, C.K. An IPT battery charger with near unity power factor and load-independent constant output combating design constraints of input voltage and transformer parameters. *IEEE Trans. Power Electron.* **2019**, *34*, 7719–7727. [CrossRef]
14. Mangu, B.; Akshatha, S.; Suryanarayana, D.; Fernandes, B.G. Grid-connected PV-wind-battery-based multi-input transformer-coupled bidirectional DC-DC converter for household applications. *IEEE J. Emerg. Sel. Top. Power Electron.* **2016**, *4*, 1086–1095. [CrossRef]
15. Baranwal, R.; Iyer, K.V.; Basu, K.; Castelino, G.F.; Mohan, N. A reduced switch count single-stage three-phase bidirectional rectifier with high-frequency isolation. *IEEE Trans. Power Electron.* **2018**, *33*, 9520–9541. [CrossRef]
16. Sha, D.; Xu, G.; Xu, Y. Utility direct interfaced charger/discharger employing unified voltage balance control for cascaded H-bridge units and decentralized control for CF-DAB modules. *IEEE Trans. Ind. Electron.* **2017**, *64*, 7831–7841. [CrossRef]
17. Iyer, V.M.; Gulur, S.; Bhattacharya, S. Small-signal stability assessment and active stabilization of a bidirectional battery charger. *IEEE Trans. Ind. Appl.* **2019**, *55*, 563–574. [CrossRef]
18. Chen, Y.-M.; Liu, Y.-C.; Wu, F.-Y. Multi-input DC/DC converter based on the multiwinding transformer for renewable energy applications. *IEEE Trans. Ind. Appl.* **2002**, *38*, 1096–1104. [CrossRef]
19. Chen, Y.-M.; Liu, Y.-C.; Wu, F.-Y. Multiinput converter with power factor correction, maximum power point tracking, and ripple-free input currents. *IEEE Trans. Power Electron.* **2004**, *19*, 631–639. [CrossRef]
20. Chen, Y.-M.; Liu, Y.-C.; Lin, S.-H. Double-input PWM DC/DC converter for high-/low-voltage sources. *IEEE Trans. Ind. Electron.* **2006**, *53*, 1538–1545. [CrossRef]

21. Chen, Y.; Liu, Y.; Hung, S.; Cheng, C. Multi-input inverter for grid-connected hybrid PV/Wind power system. *IEEE Trans. Power Electron.* **2007**, *22*, 1070–1077. [CrossRef]
22. Liu, Y.; Chen, Y. A systematic approach to synthesizing multi-input DC–DC converters. *IEEE Trans. Power Electron.* **2009**, *24*, 116–127. [CrossRef]
23. Chen, C.; Liao, C.; Chen, K.; Chen, Y. Modeling and controller design of a semiisolated multiinput converter for a hybrid PV/Wind power charger system. *IEEE Trans. Power Electron.* **2015**, *30*, 4843–4853. [CrossRef]
24. Shang, Y. Group pinning consensus under fixed and randomly switching topologies with acyclic partition. *Netw. Heterog. Media* **2014**, *9*, 553–573. [CrossRef]
25. Shang, Y. Consensus seeking over Markovian switching networks with time-varying delays and uncertain topologies. *Appl. Math. Comput.* **2016**, *273*, 1234–1245. [CrossRef]
26. Shang, Y. Resilient multiscale coordination control against adversarial nodes. *Energies* **2018**, *11*, 1844. [CrossRef]
27. Shang, Y. Consensus of hybrid multi-agent systems with malicious nodes. *IEEE Trans. Circuits Syst. II Express Briefs* **2019**. [CrossRef]